SLAC–PUB–7464
April, 1997

Fast Symplectic Mapping and Long-term Stability Near Broad Resonances*

Robert L. Warnock
Stanford Linear Accelerator Center, Stanford University, Stanford, CA 94309

J. Scott Berg
European Organization for High-Energy Physics (CERN), SL Division
CH-1211 Geneva 23, Switzerland

Abstract

Fast symplectic mapping, based on a canonical generator of the full-turn map in polar coordinates $(\mathbf{I}, \mathbf{\Phi})$, is a powerful tool to study long-term stability in large hadron storage rings. Accurate maps for realistic lattices can be constructed in a few hours on a workstation computer, and can be iterated to follow orbits for 10^7 turns in less than 4 hours. Orbits of the map can also be used in a non-perturbative construction of quasi-invariant actions. By bounding the small changes in quasi-invariants along many short orbits, one can derive conservative estimates of survival time for long orbits, for any initial condition in a region of phase space. A first quasi-invariant vector, J, arises from a canonical transformation $(I, \Phi) \to (J, \Psi)$, based on interpolation of invariant tori surrounding the origin. The variation of J is relatively large near a broad resonance. In such a region a second canonical transformation, associated with pendulum-like motion in appropriate variables, is required to produce a good quasi-invariant. This quasi-invariant is used to set a long-term bound on motion near a broad, large-amplitude resonance in a realistic model of the Large Hadron Collider (LHC). Interesting general properties of the pseudo-pendulum motion are studied.

To be published in Proceedings of the ICFA Workshop on Nonlinear and Collective Phenomena in Beam Physics Arcidosso, Italy, September 2-6, 1996, AIP Conference Proceedings

*Work supported in part by Department of Energy contract DE–AC03–76SF00515.

FULL-TURN MAP AS DYNAMICAL MODEL

For the primary dynamical description of a Hamiltonian accelerator model one relies on a symplectic tracking code. This is the best available description, but it is so expensive in computation time as to rule out detailed study of dynamical mechanisms over typical storage times in large hadron machines. Under the restriction that a realistic model of the machine is sought, there have been two responses to this situation: (a) try to find "early indicators" of instability, or devise some way of extrapolating the dynamical aperture as a function of the turn number; (b) construct a full-turn map that approximates the dynamics of the tracking code, while requiring much less time for computation of one-turn evolution.

For recent interesting work on (a) and references to earlier papers, see Ref. (1). Here we are concerned with (b), although our procedure for long-term bounds may also be included within the category of early indicators. Much of the past work on full-turn maps, especially at the SSC project (2), emphasized the representation of the map as a truncated Taylor series. One finds, however, that the violation of symplecticity in this approach is too large at amplitudes near the dynamic aperture, for the highest-order truncations used to date (3). An exactly symplectic map can be defined through a mixed-variable canonical generator (3, 4). The definition is implicit, in that each evaluation of the map requires the solution of a nonlinear equation. An explicit symplectic map may be constructed as a composition of Cremona maps with linear symplectic transformations; for instance, kicks in transverse momentum interleaved with rotations (5, 6). We prefer an approach based on the canonical generator, because the approximation theory of the scheme can be worked out in an elementary way. Correspondingly, we find an algorithm to construct the generator that is robust and allows systematic improvements in accuracy. The implicit nature of the map causes no trouble in practice, since the required solution of nonlinear equations can be done efficiently by Newton's method.

Our construction of the map generator proceeds from the viewpoint of modern numerical analysis, which emphasizes *local* approximation and interpolation, and is supported by convergence theorems that require only local smoothness of the function to be represented (7, 8, 9). By contrast, methods based on Taylor expansions often demand stronger conditions on the function, since convergence is controlled by the nearest singularity, which may be outside the region in which a representation of the function is required (6). The Taylor expansion of the generator used in Ref. (4) seems to have worked well enough in the example of the SSC, but there have been reports of other examples in which it did not succeed (10).

CONSTRUCTION OF FULL-TURN SYMPLECTIC MAP

Our numerical construction of the generator of a full-turn map was described in detail in Ref. (3) and reviewed briefly in Refs. (11, 12). For a report on later experience with the map see Ref. (13). The construction is based on data from a symplectic tracking code; namely, the results of single-turn tracking from many initial conditions. The generator $G(I, \Phi')$ of the map $(I, \Phi) \mapsto (I', \Phi')$ is expressed in canonical polar coordinates (I, Φ), which are normally action-angle coordinates of an underlying linear system, but need not be such. It is represented as a Fourier series in Φ', with coefficients that are spline functions of I.

In our first application of the method to the Large Hadron Collider (LHC), the map induced by the generator represents transverse motion in two degrees of freedom for one turn at fixed total energy. The energy is changed once per turn by a sinusoidal formula to represent synchrotron oscillations. The generator depends parametrically on the energy deviation $\delta = (E - E_o)/E_o$, and is expressed in terms of transverse coordinates centered at the δ-dependent fixed point of the four-dimensional map (3).

We have proposed various ways to validate the map (13), including the following: (a) point-by-point comparison of the orbits from mapping and tracking; (b) comparing resonances of the map and tracking in plots of Φ_1 vs. Φ_2, especially for narrow high-order resonances; (c) constructing a quasi-invariant torus of the map, and assessing its degree of invariance under tracking; (d) comparing the borders of chaotic regions for map and tracking. One might think also of comparing short-term apertures, but we have not yet made maps that are accurate at the short-term aperture, since that would require a great many Fourier modes and spline interpolation points, making it expensive in the case of large lattices.

We reach the interesting conclusion that maps for the LHC which show only modest point-by-point agreement with tracking (say one part in 10^4 at one turn) show excellent agreement with tracking under tests (b) and (c) (13). Thus, maps with relatively few Fourier modes and spline points, which can be iterated quickly, seem to provide a picture of the dynamics closely similar to that of tracking. Test (d) has not been carried out carefully to date.

One can prove analytically, at least for sufficiently small amplitudes, that the map obtained from our generator converges to the one-turn evolution given by the underlying tracking code, as the number of Fourier modes and the number of interpolation points go to infinity (14). Correspondingly, we find numerically that the point-by-point agreement between map and tracking improves steadily when more modes and interpolation points are introduced.

The use of polar coordinates to describe the map generator has a disadvantage in a region of phase space where one action variable is small and the other

large. In general the generator has a singularity at $I_i = 0$ for each component index i, and this spoils the map construction algorithm when I_j is small, but some I_k large. An analogous map construction algorithm can be written down in Cartesian coordinates, by substituting expansions in Hermite polynomials for the Fourier series (14). This scheme, not yet implemented in a code, would be free of coordinate singularities and seems to be a promising route to a global map construction.

In the following discussion the dynamical model is that provided by the map. Conclusions about long-term motion or resonances all refer to the map.

POINCARÉ SECTION $\mathcal{S}$ AT THE SYNCHROTRON PERIOD

We study a realistic model of the LHC in injection mode, for which the synchrotron period is 129.97 turns (15). We approximate this period by 130 turns, and modulate the energy by the rule

$$\delta = \delta_o \sin(2\pi n/130) \ , \tag{1}$$

where n is the turn number, with a realistic value $\delta_o = 5 \cdot 10^{-4}$. In this formulation the Hamiltonian is periodic with period $130C$ in the independent variable s, the arc length on a reference trajectory of circumference C. Thus, transverse phase space at $s = 0 \pmod{130C}$ forms a four-dimensional Poincaré section $\mathcal{S}$. It is useful to view the motion on the section $\mathcal{S}$, thus obtaining a stroboscopic picture of synchrotron oscillations. There exist invariant tori and resonances on $\mathcal{S}$, and these can be studied by methods that have already proved to be effective in the case of pure transverse motion at constant δ. Quasi-invariants on $\mathcal{S}$, which is to say quantities that return to nearly the same value each time the orbit passes $\mathcal{S}$, can be used to estimate long-term bounds on the motion.

LONG-TERM BOUNDS ON THE MOTION

Let us recall briefly the method for setting long-term bounds that was proposed and illustrated in Refs. (16) and (17). Suppose that we have made a canonical transformation $(I, \Phi) \to (J, \Psi)$ so that J on $\mathcal{S}$ is nearly invariant. Let Ω be an open region in the J_1, J_2 plane, and $\Omega_o \subset \Omega$ a proper subregion. Define ΔJ as the minimum Euclidean distance from Ω_o to the boundary of Ω. Let δJ be an upper bound for the absolute value of the change of J during p synchrotron periods, for any orbit with initial action $J(0)$ in Ω; here any initial angle $\Psi(0)$ is allowed. Then J on an orbit with $J(0) \in \Omega_o$ cannot leave

Ω in fewer than $p\Delta J/\delta J$ synchrotron periods. If n_s is the number of turns per period, then we have stability for N turns (in the sense of J staying within Ω when $J(0) \in \Omega_o$), where

$$N = pn_s\Delta J/\delta J \ . \tag{2}$$

In a numerical realization of this simple argument a principal problem is the matter of how to determine δJ. One possibility is to use interval arithmetic (18), which can provide rigorous error bounds for numerical calculations. Berz and Hoffstätter (19) carried out such a plan in a formulation based on Taylor series maps, giving results for some accelerator models. Recently, Berz (20) has reported progress on a general and efficient way of implementing interval arithmetic, using controlled "models" of the functions involved. This approach might be adapted to handle our type of map.

Interval arithmetic is likely to be expensive in computation time whenever it furnishes a close upper bound on the maximum of a function. A less costly approach is to use some sort of Monte Carlo sampling, which is known to be more efficient than raster-based sampling in high dimensional problems. Although this could not claim the rigor of interval arithmetic, it may very well provide a better guess for the minimum δJ in a given computation time. Inevitably, the task in studying long-term stability in accelerators is to provide a sophisticated guess, not to prove theorems, since our Hamiltonian is itself a guess.

The traditional Monte Carlo method for computing integrals converges as $1/\sqrt{n}$, where n is the number of samples, irrespective of the dimension of the problem. This estimate has a probabilistic character, however, and need not be literally valid when the method is realized through pseudo-random numbers on a computer. The quasi-Monte Carlo method, based on deterministic "quasi-random sequences" (21), can give $\log n/n$ convergence in a strict (not probabilistic) sense. The "method of good lattice points" (22) is a related method for integration of periodic functions. Adaptation of quasi-Monte Carlo or good lattice points to maximization rather than integration may provide an interesting approach to the problem of finding a minimum upper bound δJ. To date we have used simple sampling with pseudo-random numbers, together with some knowledge of the specific character of our function, to arrive at estimates that seem plausible.

There are certain aspects of our evaluation of N in Eq. (2) that make the task easier than might be expected. First, one finds in typical cases that estimates of δJ increase slowly, if at all, with increasing p. Thus, if one can afford the computation to get δJ for large p, the desired large value of N can be obtained. Second, one finds that the algebraic change dJ in J over p periods, including sign, fluctuates about an average value that is about two

orders of magnitude smaller than $|dJ|_{max}$. Here we refer to fluctuations within an ensemble of orbits with the same p, or within a single orbit for increasing p. This suggests that even if our estimate of δJ is considerably less than a true value, our value of N will still be a conservative estimate. That is, the probability of many changes dJ of maximum magnitude adding coherently to bridge the gap between Ω_o and Ω is extremely small. Third, it appears that $dJ(J(0), \Psi(0))$ has the same general character as a function of $(J(0), \Psi(0))$ for any value of p. It has a lot of oscillations as a function of $\Psi(0)$, but the amplitude and wavelength of the oscillations seem to be fairly uniform over phase space and with respect to p, with no evidence of peaks a great deal larger than average, or wavelengths much smaller than average. This leads to the idea of using results for small p as a guide on how to extrapolate from small random samples to large, even when p is large. Some experience with this trick is reported later in this paper.

CONSTRUCTION OF QUASI-INVARIANTS ON $\mathcal{S}$

We determine quasi-invariants from orbits of the map, just as we used orbits of tracking to construct the map. This non-perturbative method succeeds even at large amplitudes close to chaotic regions, and in general has a greater scope and reliability than perturbation theory, while being competitive in computation time. An important advantage of our method in the present problem is that it allows us to find invariants of the map over a synchrotron period of 130 turns. This would not be possible in perturbation theory without an explicit construction of a 130-turn Taylor series map, a task that would be quite difficult.

The particular method that we have used to determine invariants from orbits is based on polar coordinates, and suffers from the coordinate singularity noted above when one action variable is small while the other is large. In such a case the method is not a good substitute for perturbation theory in Cartesian coordinates. It is likely, however, that a modified method based on orbit data can be devised to handle the general case.

Let $\mathcal{P}_n = \{(I, \Phi)^{(i)}, i = 0, 1, \cdots, n\}$ be a sequence of $n+1$ points on the Poincaré section $\mathcal{S}$, namely the first $n+1$ points at which a single orbit crosses $\mathcal{S}$. For a large set of initial conditions $(I, \Phi)^{(0)}$ the points of the orbit will lie on an invariant torus, which can be represented as a Fourier series for I as a function of Φ:

$$I = \sum_m I_m e^{im\cdot\Phi} \ . \tag{3}$$

This equation may also be stated in terms of a generating function $\mathcal{G}(J, \Phi)$ of a canonical transformation $(I, \Phi) \mapsto (J, \Psi)$, where J is an invariant of the

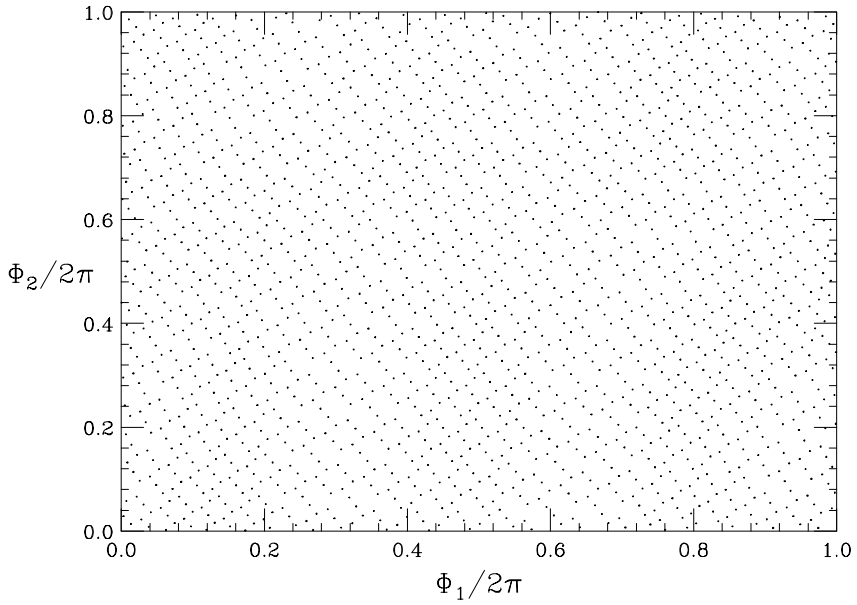

FIGURE 1. A plot of Φ_2 vs. Φ_1 for an orbit on a quasi-invariant torus

motion on $\mathcal{S}$. Developing $\mathcal{G}$ in a Fourier series with coefficients $g_m(J)$, we have

$$I = J + \mathcal{G}_\Phi(J,\Phi) = J + \sum_m img_m(J)e^{im\cdot\Phi} \ , \tag{4}$$

where J is the zero mode (the term for $m = 0$). The value of J serves as a label to distinguish various tori. The Fourier coefficients may be determined from the sequence $\mathcal{P}_n$, to arbitrary accuracy at sufficiently large n. The determination is not a standard problem of numerical Fourier analysis, however, since the points $\Phi^{(j)}$ are distributed unpredictably while usual methods like the FFT require data on a uniform grid. A stable method of dealing with this problem is to take the values of I on a uniform grid in Φ as the unknowns in place of the coefficients I_m. With a number of cells in the i-th dimension equal to $2M_i + 1$, where M_i is the maximum mode number for that dimension, we choose the number of orbit points n to be so large that at least one $\Phi^{(j)}$ lies in each cell. Retaining just one point per cell, we then obtain a well-conditioned system of linear equations to determine the values of I on the grid; from those the Fourier coefficients can be calculated by an FFT. In the case of a resonant orbit there will be regions of Φ space that are never visited by the orbit, hence cells that never contain an orbit point if M_i is sufficiently large. Then the method fails, as it must, since the orbit does not lie on a surface of the form (3). At large amplitudes one also finds chaotic orbits, which may provide at least one point per cell if M_i is not too big. These are easily recognized visually, if not mathematically. The points tend to cluster and do not line

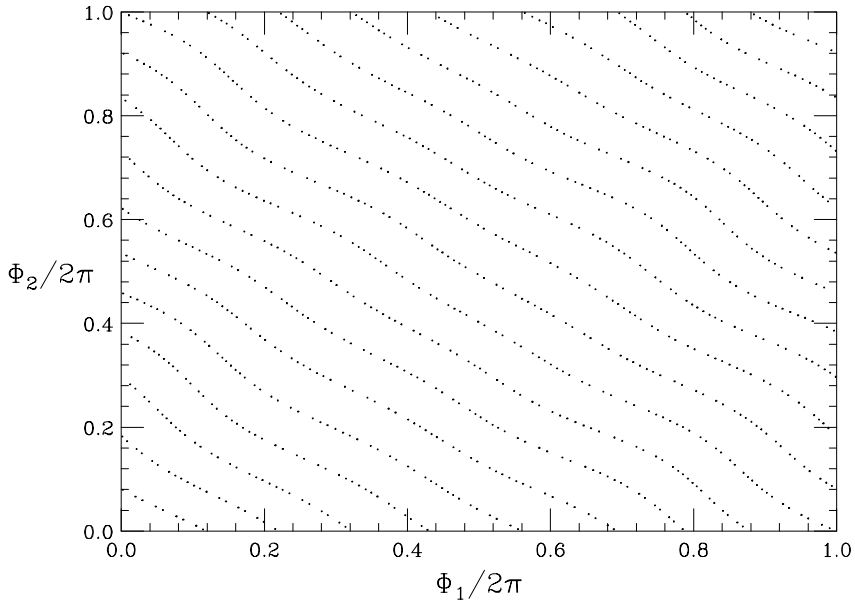

FIGURE 2. A plot of Φ_2 vs. Φ_1 for an orbit on resonance

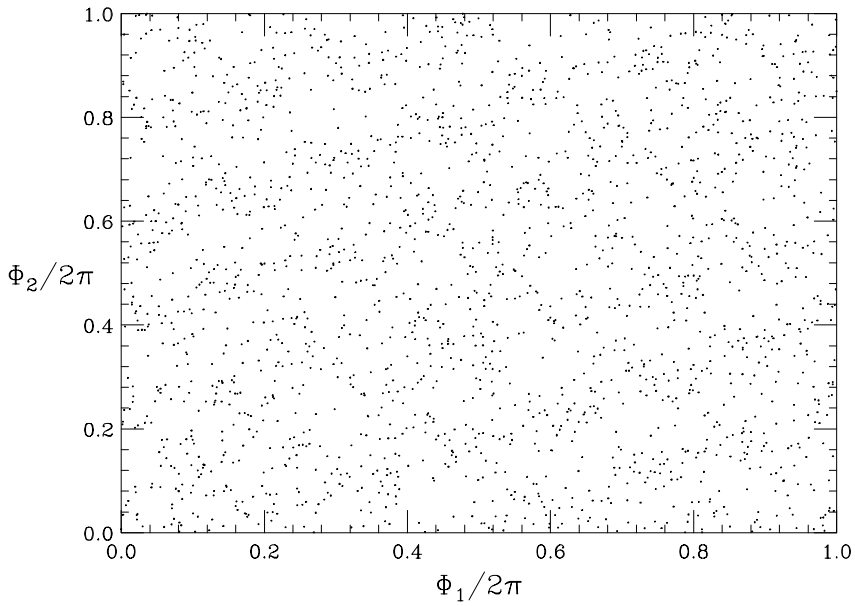

FIGURE 3. A plot of Φ_2 vs. Φ_1 for a chaotic orbit

up in the orderly manner that one sees in the case of nearly invariant tori. The calculation of the Fourier coefficients may go through without difficulty, but the coefficients do not fall off with increasing m, and the resulting surface is far from being invariant. Indeed, the failure of invariance for a torus con-

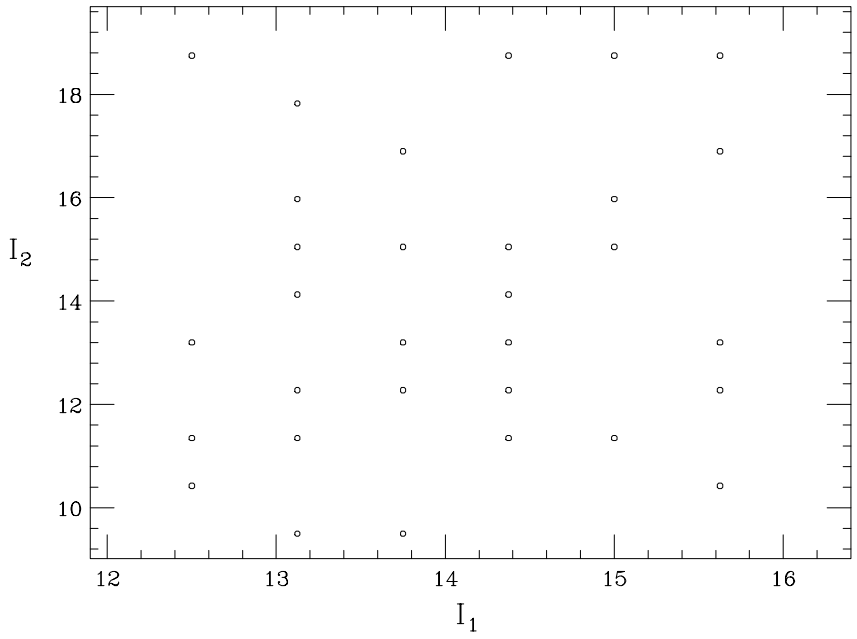

FIGURE 4. Initial actions on a 6×11 grid with filling fractions greater than 41% in 2000 periods. The number of cells in Φ space is 51^2, corresponding to a maximum Fourier mode number of 25 in either dimension.

structed from orbit data may be regarded as a mathematical test for chaos. Figure 1 shows a plot of Φ_2 vs. Φ_1 for an orbit on a nearly invariant torus. For comparison, Fig. 2 shows a resonant orbit, and Fig. 3 a chaotic orbit.

For the LHC, the length of orbit required to construct a torus with 15 Fourier modes in each direction is typically 5000 to 10000 synchrotron periods. The computation time is 17 to 34 minutes on an IBM RS6000-590 workstation, when the map is like that described in (23). A lot of time can be wasted, however, in futile attempts to fit tori to resonant orbits. To facilitate the finding of good tori, we do a survey of phase space, testing a set of orbits on a grid of initial conditions. Each orbit on the grid if followed for a relatively small number of periods, say 2000, and the fraction of cells in Φ_1, Φ_2 space that are visited by the orbit is recorded. Those orbits that hit a large fraction of the cells (say more than 40%) are good candidates for tori, while those that hit only a small fraction (say less than 25%) are almost certainly resonant. Such a survey at least reduces the amount of human work required, even if it takes a fairly long computer run. In Fig. 4 we show a typical survey, showing those initial actions that give a filling fraction greater than 41% for orbits of 2000 periods, for cells in Φ space corresponding to a maximum Fourier mode number of 25 in either dimension. As expected, the phase space is quite inhomogeneous with respect to this aspect of orbits.

In a region devoid of large-scale chaos, one may usually construct a num-

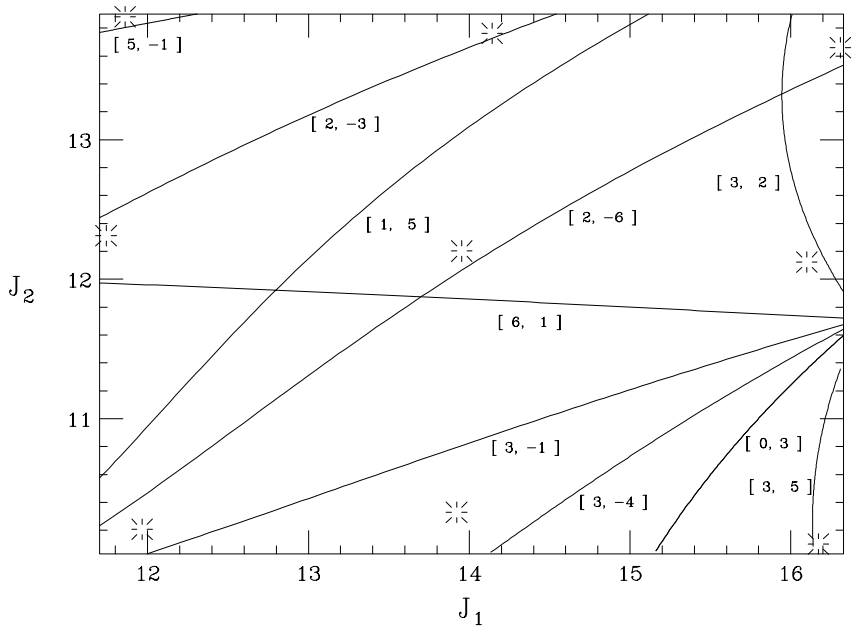

FIGURE 5. Resonance lines in a region of the J-plane, for all resonances with $|m_1| + |m_2| \leq 8$. J is in units of 10^{-8}m. The stars mark the values of J on the original fitted tori used to define the first canonical transformation.

ber of tori of the form (3), changing initial conditions if necessary to dodge resonances. For instance, one may find tori for a roughly Cartesian grid of initial conditions $I^{(0)}$ in the I-plane, all with $\Phi^{(0)} = 0$. These tori may then be interpolated smoothly in J, for instance by cubic spline interpolation of the Fourier coefficients $g_m(J)$ for C^2 smoothness. This gives the generator $G(J, \Phi)$ of a canonical transform $(I, \Phi) \mapsto (J, \Psi)$ that is rigorously defined in an open domain of J space. The quasi-invariant J will be nearly constant on $\mathcal{S}$ as a function of turn number, at least on the original tori that were fitted to orbits. On interpolated tori J may be less constant, particularly if the interpolation forms a bridge over a strong resonance. The canonical transformation may partially normalize the motion, taking out the principal, global distortion of the underlying linear motion, while leaving the local effect of a resonance. It is this residual effect of a resonance that we wish to explore in the following.

Each fitted torus has a tune ν that is rather well-defined, since the new phase angle advances by a nearly constant amount $2\pi\nu$ per turn. (Note that a "turn" may here refer to a full synchrotron period, 130 turns in our LHC model, if synchrotron oscillations are accounted for by the method described above.) These tunes on fitted tori can be interpolated in J, to give a smooth function $\nu(J)$. If the interpolation is well-behaved, in the sense of providing a well-defined inverse function $J(\nu)$, then we can map resonant tune lines, $m \cdot \nu = p,\ p =$ integer, into the J-plane.

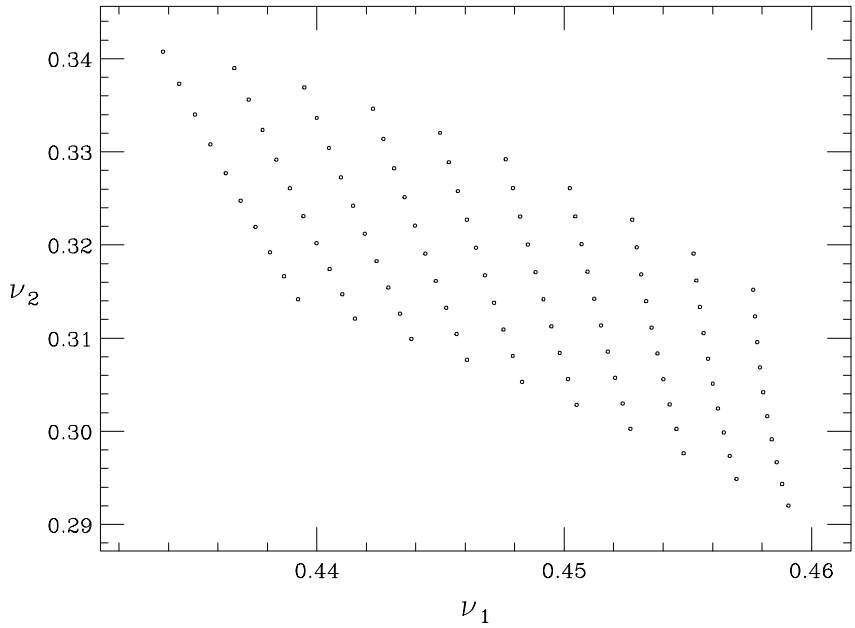

FIGURE 6. The tune $\nu(J)$ for values of J on a rectangular grid in the region of Fig. 5.

Such a map for region of LHC J-space is shown in Fig. 5, for all resonances up to order 8. The corresponding canonical transformation was based on interpolating 9 fitted tori, on a 3×3 grid indicated by points marked in the figure with an asterisk. This interpolation bridges over a strong $(6, 1)$ resonance. We shall see that the $(6, 1)$ makes itself clearly felt over the whole region of J-space of the plot and more. Notice that this is quite a big region, corresponding to about a 30% change in J. The other resonances shown in Fig. 5 have relatively minor effects, almost unobservable, even though some are of low order. The presence of many low-order resonances that are quite weak can be traced to the fact that we are here dealing with tunes for 130 turns.

Although an interpolation of fitted tori and tunes can usually be made, it may happen that $\nu(J)$ is not a nice function and the inverse $J(\nu)$ does not exist. In that case the picture of a partial normalization leaving the local effect of a resonance is simply not valid, and an analysis like that pursued in the following sections is not possible. This has been our experience to date in regions very close to large-scale chaos. It may sometimes be possible to retrieve such a picture by working in a smaller region of phase space, or changing the choice of fitted tori. A good case, that corresponding to Fig. 5, is illustrated in Fig. 6, which shows the behavior of $\nu(J)$ on a uniform grid in J-space. The figure clearly suggests that the inverse function $J(\nu)$ exists, and that is confirmed by an accurate calculation of the inverse by Newton's method.

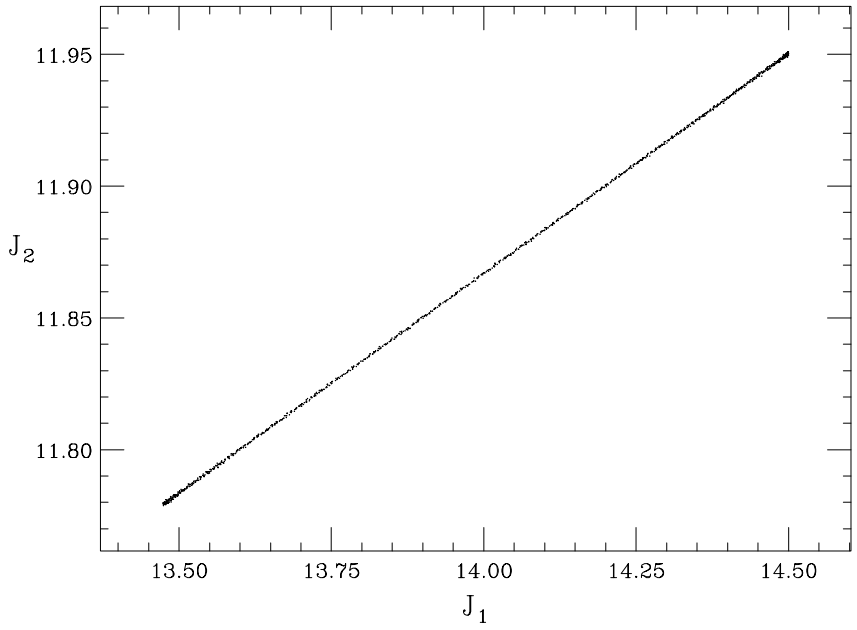

FIGURE 7. A plot of J_2 vs. J_1 for an orbit in the [6,1] resonance region. Units: 10^{-8}m.

PENDULUM-LIKE MOTION NEAR A BROAD RESONANCE

When we attempt to estimate the maximum change in J in the region of Fig. 5, we find that it is considerably larger, by almost a factor of 100, than the change for orbits starting on the original fitted tori that determined the canonical transformation. This is due to the strong $(6,1)$ resonance that lies between the fitted tori. It is difficult to get suitable long-term bounds with such large variations, so we are led to a detailed examination of the resonance in the hope of finding a new, more constant quasi-invariant. A plot of J_2 vs. J_1 along an orbit beginning near the resonance shows points lying close to a line segment, as we see in Fig. 7. This suggests that the motion may follow an isolated-resonance model, in which the Hamiltonian has the form

$$H(K_1, K_2, \chi_1, s) = \sum_p h_p(K_1, K_2) e^{ip(m\chi_1 - ns/(130C))} \ , \tag{5}$$

where

$$K_1 = \hat{m} \cdot J = \hat{m}_1 J_1 + \hat{m}_2 J_2 \ , \quad \chi_1 = m \cdot \Psi = m_1 \Psi_1 + m_2 \Psi_2 \ , \tag{6}$$

$$K_2 = \hat{m} \times J = \hat{m}_1 J_2 - \hat{m}_2 J_1 \ , \quad \chi_2 = m \times \Psi = m_1 \Psi_2 - m_2 \Psi_1 \ , \tag{7}$$

$$\hat{m}_i = m_i (m_1^2 + m_2^2)^{-1/2} \ , \quad i = 1, 2 \ . \tag{8}$$

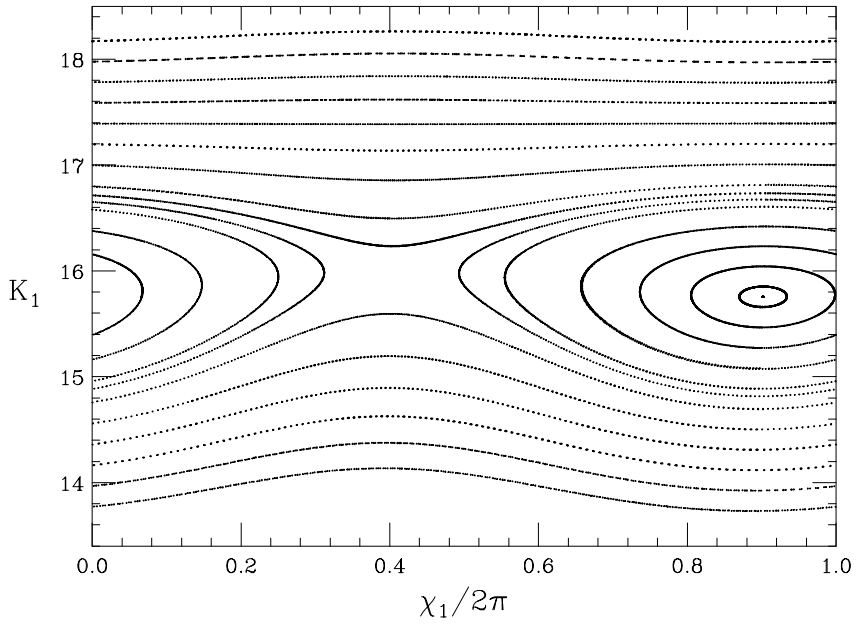

FIGURE 8. A plot of K_1 vs. $\chi_1 \pmod{2\pi}$ for several orbits in the [6,1] resonance region. All orbits have the same initial value of K_2. Units: 10^{-8}m.

Since H is independent of the angle χ_2, the conjugate action K_2 is constant on orbits of H, which is to say that the motion in the J_1, J_2 plane is along a line parallel to the vector m. This agrees approximately with Fig. 7, if $m = (6, 1)$. Note that this simple behavior cannot be seen in the original variables. A plot in the I_1, I_2 plane shows some sort of complicated oscillatory motion.

Further confirmation of the isolated resonance model is seen when we plot several orbits on the section $\mathcal{S}$ at the same initial value of K_2, graphing K_1 vs. $\chi_1 \pmod{2\pi}$, as in Fig. 8. We see pendulum-like motion, which we classify as *rotation* when $\chi_1 \pmod{2\pi}$ ranges over the full interval $[0, 2\pi]$ or *libration* (island motion) when it oscillates over subintervals of $[0, 2\pi]$. Obviously we cannot have perfect pendulum motion, since the system is still non-integrable. The departure from the ideal is seen in small fluctuations of K_2 along an orbit, as shown in Figs. 7 and 9, or by examining the apparent curves of Fig. 8 on a finer scale to reveal that the points actually scatter about an averaging curve, with a spread similar in magnitude to that of K_2 in Fig. 9.

A closer investigation shows further interesting departures from pure pendulum motion. An attempt to find the elliptic fixed point results in a small cloud of points in the $K_1 - \chi_1$ plane with some minimum spread, as shown in Fig. 10. We have tried to determine whether this cloud represents a projection of some more exact structure in a higher dimensional space. For instance, we might be seeing a projection of a curve with χ_2 as curve parameter. To check this idea, we compute a long orbit (about 40000 synchrotron periods), and

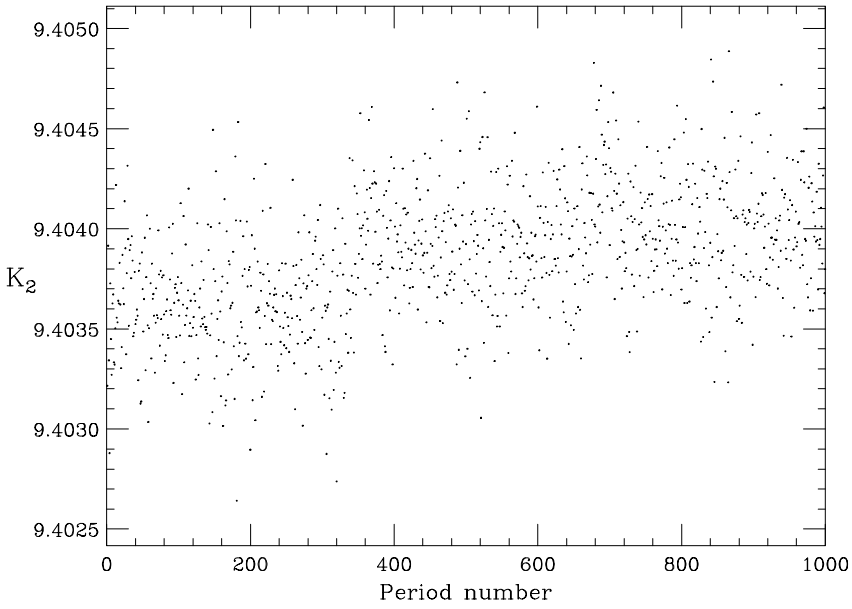

FIGURE 9. A plot showing fluctuations of K_2 along a single orbit in the [6,1] resonance region. Units: 10^{-8}m.

plot only points for which $\chi_2 \pmod{2\pi}$ falls into a small interval. We find that the picture is still very similar to that of Fig. 10, the magnitude of the spread being about the same. This seems to rule out the proposed structure, at least if it were 2π-periodic in χ_2. Next we tried looking at points for which K_2 falls into a small interval, again finding a spread similar to that of Fig. 10. The conjecture here was that for a small range of K_2 the orbit might resemble more closely an isolated-resonance orbit. Finally, we tried simultaneous restrictions on both of the aforementioned variables, and in that trial we did see some structure, typically a few small ellipses, fuzzy and overlapping, as in Fig. 11. By a careful tuning of the interval of K_2, this picture may be changed to two ellipses, or to one, or to no points at all. The case of two ellipses is shown in Fig. 12. For the case of a single ellipse, we moved the short interval of χ_2, unchanged in length, while leaving the interval of K_2 unchanged, and again found several overlapping ellipses.

Turning attention to the region where a hyperbolic fixed point would exist in pure pendulum motion, we find that separatrix-like rotation curves are well-defined (modulo the scatter displayed in any of our "curves") over a time of about one pendulum rotation period. The curves follow different courses over successive periods, however, approaching more or less closely an imagined (but nonexistent) hyperbolic point, as is seen in Fig. 13. It is as though the energy of the pendulum were modulated, being changed a little from one period to the next. If we adjust the initial condition of the orbit to approach the imagined

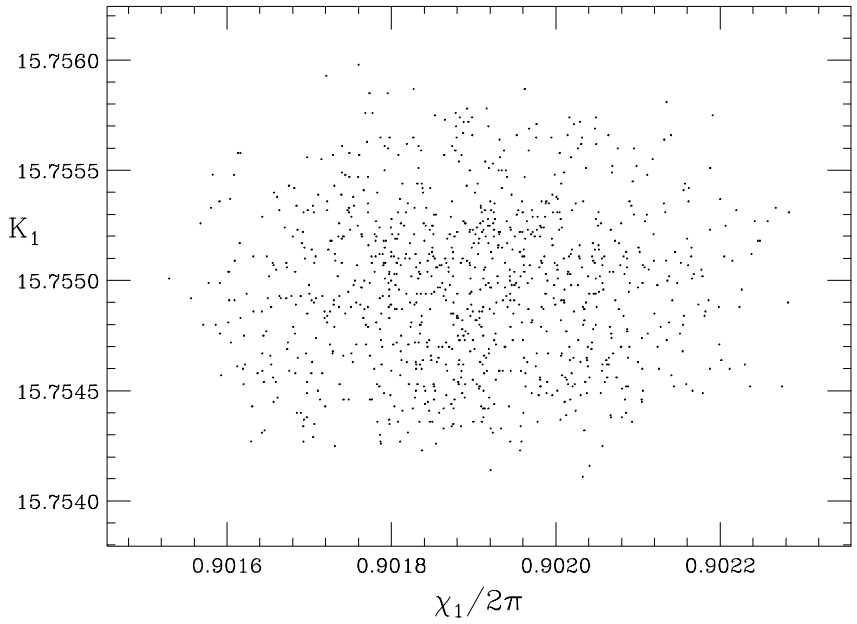

FIGURE 10. The points corresponding to the "elliptic fixed point" of Fig. 8 plotted on a larger scale.

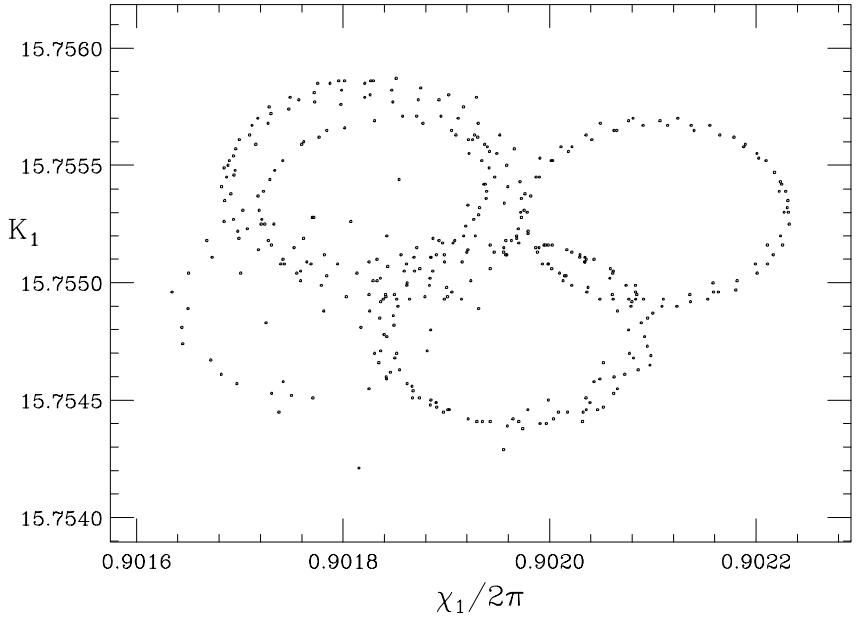

FIGURE 11. Points corresponding to the smeared "elliptic fixed point" of Fig. 10, but with simultaneous cuts in K_2 and χ_2; namely, $9.4023 < K_2 < 9.4028$, $0.6 < \chi_2/2\pi < 0.7$.

hyperbolic point more closely, we find orbits in which rotations change into librations, and vice-versa. Over a time of about one period, the motion has

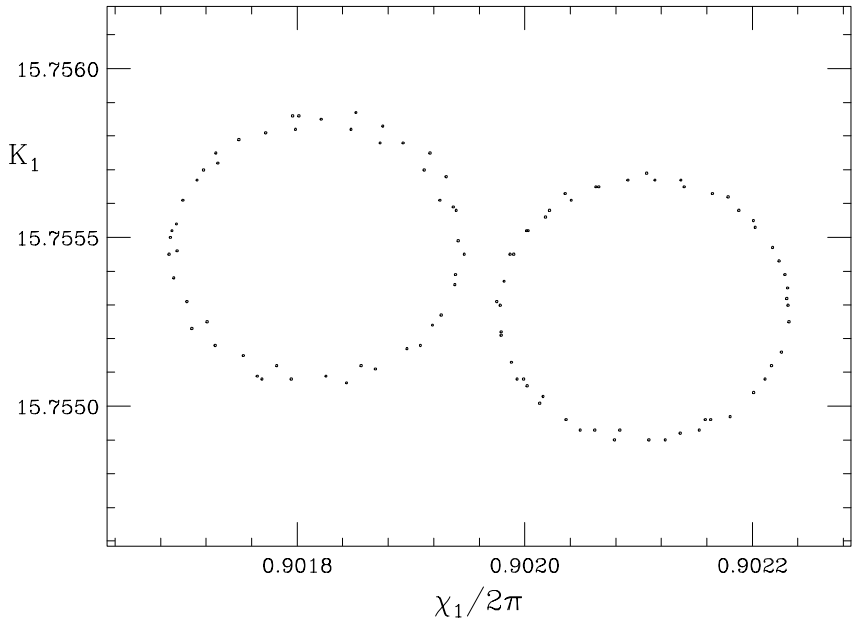

FIGURE 12. Points corresponding to the smeared "elliptic fixed point" of Fig. 10, but with simultaneous cuts in K_2 and χ_2; namely, $9.4025 < K_2 < 9.4026$, $0.6 < \chi_2/2\pi < 0.7$.

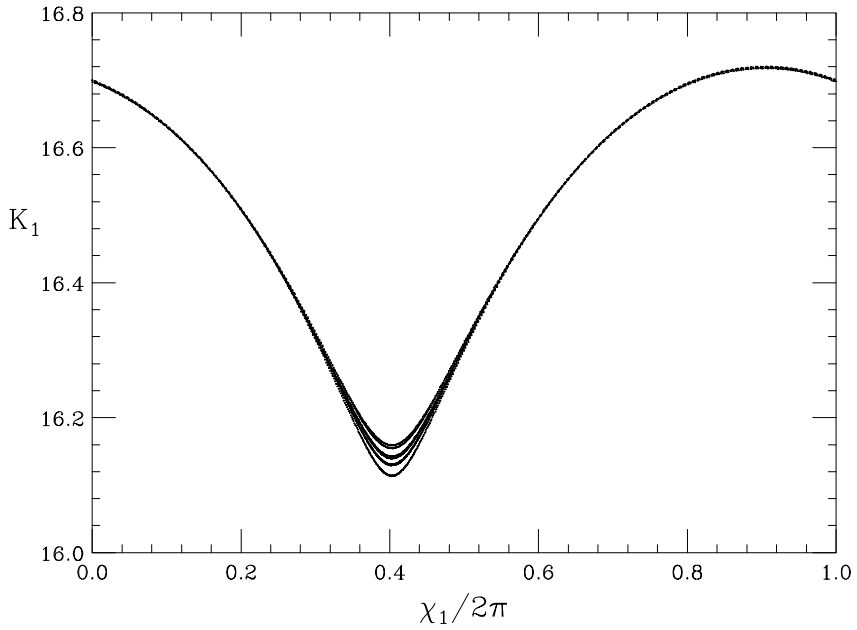

FIGURE 13. Points on a single orbit near an imagined "hyperbolic fixed point". Over a time of about one pendulum period a curve is well-defined (modulo the minimum smear seen in any of the pendulum curves), but takes a different course from one pendulum period to the next.

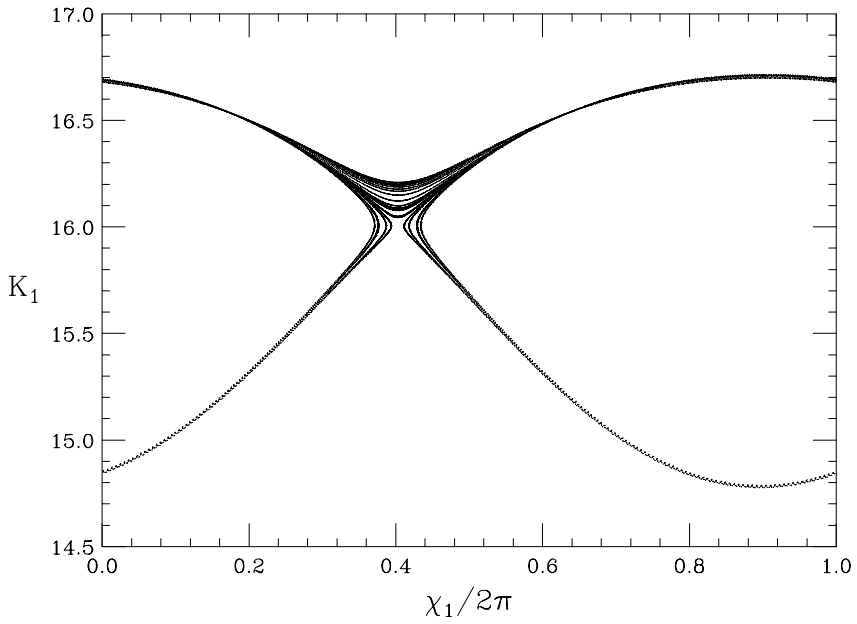

FIGURE 14. Points on a single orbit near an imagined "hyperbolic fixed point". In comparison to Fig. 13, the initial condition is adjusted to bring the orbit slightly closer to the "fixed point". Over a time of about one pendulum period the orbit has either rotational or librational character, and shifts from one to the other in apparently random fashion.

one character or the other. Fig. 14 shows an orbit that made four transitions between the two types of motion, and then several rotations. On a longer time interval, following that of the plot, it made many more rotations but eventually went into libration again. These "changes in pendulum energy" seem to occur in random patterns, and that is the only manifestation of "chaos" beyond the small scatter in the curves during a pendulum period. It is of course conceivable that the changes have some pattern or periodicity that we have not yet noticed.

The pendulum period we refer to in the experiments near the hyperbolic point is rather long, around 700 synchrotron periods. Far from the hyperbolic point in the rotation region there are similar but less pronounced shifts in the orbits over a rotational period, the latter of course now being somewhat shorter. Slow time evolution of fairly well-defined structures might also account for the existence of several ellipses in Fig. 11.

QUASI-INVARIANTS NEAR A STRONG RESONANCE

One quasi-invariant that is suitable for our purposes is K_2. A second is associated with those rotation orbits that are not too close to separatrix-like orbits. As we have seen, the orbits do not define exact curves, always exhibiting

a slight scatter about an imagined averaging curve. To define quasi-invariants precisely, we make a least-squares fit of K_1 to a Fourier series in χ_1, for each of several orbits that all have the same initial value $K_2(0)$ of K_2, and the same initial angles, say $(\chi_1(0), \chi_2(0)) = (0, 0)$. We repeat this step for several values of $K_2(0)$, and finally interpolate the full set of Fourier coefficients by cubic splines to obtain a smooth foliation of a region by surfaces represented as Fourier series. Convenient variables in which to interpolate are $K_1(0)$ and $K_2(0)$, so that we come out with a series

$$K_1 = \sum_n a_n(K_1(0), K_2(0)) e^{in\chi_1} \ , \tag{9}$$

where the coefficients a_n have continuous second derivatives. For a point $(K_1, K_2, \chi_1, \chi_2)$ on an arbitrary orbit in the region of phase space covered by our foliation, we choose the quasi-invariants to be K_{10} and K_2, where K_{10} is the solution of the equation

$$K_1 = \sum_n a_n(K_{10}, K_2) e^{in\chi_1} \ . \tag{10}$$

In practice the solution of (10) is easily obtained by Newton's method, using the initial value of K_1 on the orbit in question as the zeroth iterate.

In place of K_{10} one could as well use the more conventional action variable, the coefficient of the zero mode in (9):

$$\langle K_1 \rangle = \frac{1}{2\pi} \int_0^{2\pi} K_1 d\chi_1 \ . \tag{11}$$

The computations are much more convenient with K_{10}, however, and the latter has substantially the same behavior as $\langle K_1 \rangle$. Both choices measure a drift in the center of oscillation along the direction of m, while K_2 measures a drift perpendicular to m.

We have now defined quasi-invariants for the outer rotation orbits on either side of a wide resonance island. We shall find that these quantities are sufficiently constant so as to ensure that any orbit that finds its way into an outer rotation region will stay there for a very long time, at least in the example under discussion. What happens in the region inside and near the island is then irrelevant for long-term behavior, since an orbit in that region will either stay there or move into a rotation region and then be trapped for a long time. In other words, in a "worst case scenario" we can assign zero time to cross the island.

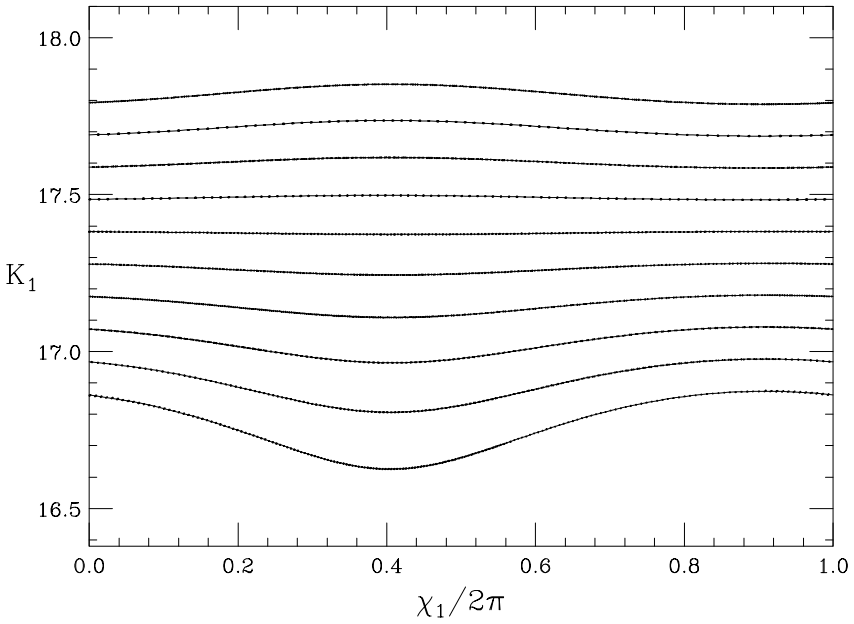

FIGURE 15. Data for 10 rotational pendulum orbits and the curves obtained by fitting them to Fourier series with 8 modes. The orbits all have the same initial value of K_2. The data are barely distinguishable from the curves at the resolution of the plotter.

LONG-TERM BOUND NEAR A BROAD, LARGE-AMPLITUDE RESONANCE

We now consider long-term behavior of orbits in the region of J-space shown in Fig. 5. Through long-term mapping of single orbits we estimate roughly that this region is at 80% of the long-term (10^6 turn) dynamic aperture. (Here we measure the distance to the aperture in terms of the amplitude, $(J_1^2 + J_2^2)^{1/4}$, which is roughly proportional to the transverse displacement of the particle.) We have chosen this large-amplitude region to test our method under difficult conditions of practical interest. These conditions are probably close to the extreme for which our method can predict stability over times comparable to desired storage times. At amplitudes a bit larger the motion becomes chaotic and good quasi-invariants apparently do not exist. We set up a least-squares fit to rotation orbits as described in the previous section, obtaining a series as in Eq.(9) over a domain as follows, in units of 10^{-8} meters:

$$15.1 < K_1(0) < 16.0 \ , \qquad 9.40 < K_2(0) < 10.1 \ . \tag{12}$$

We tried both a 4×4 and a 10×10 uniform Cartesian grid in the $(K_1(0), K_2(0))$-plane as the set of points to interpolate. We used the 10×10 grid finally, although the quasi-invariants it provided were not substantially more constant than those for the 4×4. This indicates that the limit in quality of quasi-

invariants cannot be overcome by finer interpolation. We used 8 Fourier modes in Eq.(9), after finding that a larger mode set did not improve the fit or the quality of quasi-invariants. Fig. 15 shows a typical fit to 10 orbits for a fixed $K_2(0)$. Note that the rotational orbits do not straighten out completely with increasing distance from the island, unlike the case of real pendulum motion, and they may be concave upward or downward. The location of the region in which they are fairly straight will depend on the choice of the fitted tori that defined our first canonical transformation.

Using pseudo-random numbers, we made an ensemble of 2040 randomly chosen initial conditions in (J, Ψ) space, allowing the full range of $\Psi(0) \in [0, 2\pi]^2$, but restricting $J(0)$ so that $K(0)$ lay in the rectangle (12). We followed an orbit from each initial condition for 2000 synchrotron period, and found the following ensemble maxima for changes in absolute values of quasi-invariants over 2000 periods (in units of $10^{-8}m$):

$$\delta K_{10} = 9.9 \cdot 10^{-3} \ , \qquad \delta K_2 = 1.7 \cdot 10^{-2} \ . \tag{13}$$

The corresponding ensemble average changes including sign, $\langle dK_{10} \rangle$ and $\langle dK_2 \rangle$, are smaller in magnitude by about a factor of 100. Because of the relatively small sample, we think that that the results are an underestimate, and seek a way to make a correction. As mentioned in Section 4, a way to correct is to look at the behavior of the changes versus sample size for a map over 1 synchrotron period instead of 2000. This seems reasonable, since the function to be maximized seems to be qualitatively similar for 1 and 2000 periods. Fig. 16 and 17 show typical sections of the two functions, in which one initial angle varies while the other three variables are fixed. Computing an ensemble of 240000 one-period orbits, and comparing to an ensemble of 2000 one-period orbits, we get an increase of about 30% in the ensemble maxima of δK. Moreover, the data suggest that the 240000 samples give a good estimate for the true maxima of the one- period map, since large increases in the maxima occur only over the first few thousand samples. After 50000 samples we found no change at all. In view of these results, and the encouraging circumstance that ensemble averages including sign are much smaller than maxima, we think it safe to increase the estimates (13) for 2000 periods by 30% and base long-term bounds on the resulting values. For orbits with $K_1(0), K_2(0)$ near the center of the rectangle (12) the minimum distances to the boundary of the rectangle in the two directions are $\Delta K_1(0) = 0.45, \Delta K_2(0) = 0.35$. Since $p = 2000,\ n_s = 130,\ \delta K_{10} = 0.013,\ \delta K_2 = 0.022$, we see from Eq. (2) that such orbits cannot leave the rectangle in fewer than $4 \cdot 10^6$ turns. The required stability time for injection in the LHC corresponds to $7 \cdot 10^6$ turns.

Thus, we have given a "proof of principle" for our method. We have shown that very conservative predictions of stability in the LHC can be made for times comparable to the injection time, even in the neighborhood of a broad, large-amplitude resonance not far from the estimated dynamic aperture. Needless

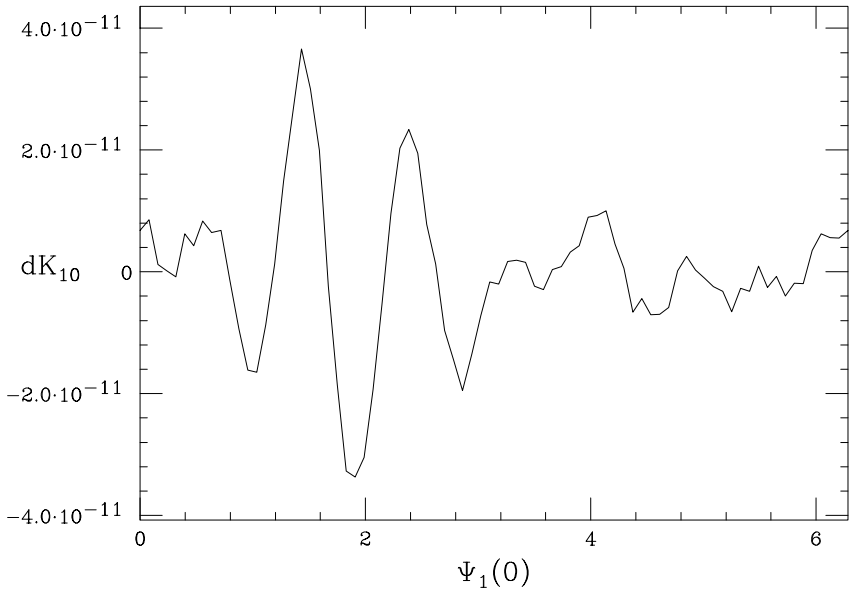

FIGURE 16. The change dK_{10} in K_{10} over 2000 synchrotron periods versus initial angle $\Psi_1(0)$ with other initial coordinates (randomly chosen) held fixed. dK_{10} in meters.

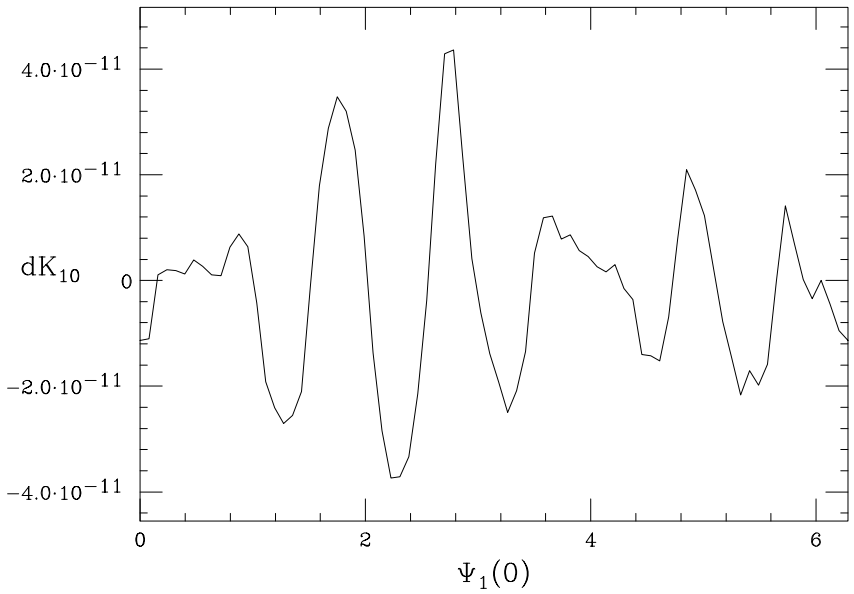

FIGURE 17. The change dK_{10} in K_{10} over 1 synchrotron period versus initial angle $\Psi_1(0)$ with other initial coordinates (randomly chosen) held fixed. dK_{10} in meters.

to say, corresponding predictions for a big region of phase space would require much more extensive computations along the same lines. These computations lend themselves well to parallel computation, since the many short orbits required for evaluation of $\delta K's$ could be followed in parallel operations.

DIRECT TEST OF LONG-TERM PREDICTIONS BY MAPPING

We have tested the prediction of stability of the previous section by direct mapping of long orbits. For instance, we have followed 9 orbits for 10^7 turns each, the orbits having initial conditions near the center of the domain (12). As expected, every orbit stayed near its starting point in K_{10}, K_2 space, in fact with much less change than the bounds (13) would suggest.

ACKNOWLEDGMENTS

Some of the ideas in this paper arose in enjoyable conversations with James Ellison, Ezio Todesco, Giorgio Turchetti, and Étienne Forest. Our calculations were made possible by the kind help of Frank Schmidt and Étienne Forest, who provided a lattice and tracking code for the LHC. This work was supported in part by U. S. Department of Energy contract DE–AC03–76SF00515.

REFERENCES

1. Giovannozzi, M., Scandale, W., and Todesco, E., LHC Project Report 45, CERN, Geneva, 1996 (submitted to *Particle Accelerators*).
2. Yan, Y. T. *et al.*, eds., *Accelerator Physics at the Superconducting Supercollider*, *AIP Conference Proceedings* **326**, 1995; Forest, É., Berz, M., and Irwin, J., *Particle Accelerators* **24**, 91 (1987).
3. Berg, J. S., Warnock, R. L., Ruth, R. D., and Forest, É., *Phys. Rev. E* **49**, 722 (1994).
4. Yan, Y., Channell, P., and Syphers, M., Superconducting Supercollider Report SSCL-Preprint-157, 1992 (unpublished).
5. Irwin, J., Superconducting Supercollider Report SSC-228, 1989 (unpublished), and *AIP Conference Proceedings* **326**, p. 662.
6. Abell, D. T., Ph.D. Thesis, University of Maryland, 1995.
7. Rivlin, T. J., *An Introduction to the Approximation of Functions*, New York: Dover, 1969.
8. de Boor, C., *A Practical Guide to Splines*, New York: Springer, 1978.
9. Schumaker, L. L., *Spline Functions: Basic Theory*, New York: Wiley, 1981.
10. Forest, É., private communication.
11. Berg, J. S., Warnock, R. L., Ruth, R. D., and Forest, É., in *AIP Conference Proceedings* **297**, ed. Ryne, R., 1994, p. 413.
12. Warnock, R. L., and Berg, J. S., SLAC-PUB-95-7045, 1995, to be published in *Proceedings of NATO Advanced Study Institute on Hamiltonian Systems with Three or More Degrees of Freedom*, Catalunya, Spain, June 19-30, 1995.
13. Warnock, R. L., and Berg, J. S., in *Proceedings of LHC95 - Second International Workshop on Single Particle Effects in Large Hadron Colliders*, Montreux, October 15-21, 1995, eds. Keil, E., and Schmidt, F., published in *Particle Accelerators*, **54** Numbers 2-4, **55** Numbers 1-4, 1996.

14. Warnock, R. L., and Ellison, J., *Convergence of A Fourier-Spline Representation of the Poincaré Map*, in preparation.
15. A lattice description of the LHC (as it existed in 1995) was provided by Frank Schmidt. A tracking code with this lattice was given to us by Étienne Forest.
16. Warnock, R. L., and Ruth, R. D., *Phys. Rev. Letters* **66**, 990 (1991).
17. Warnock, R. L., and Ruth, R. D., *Physica D* **56**, 188, 1992.
18. Rall, L. B., *Automatic Differentiation: Techniques and Applications*, *Lecture Notes in Computer Science* **120**, Berlin: Springer, 1981.
19. Hoffstätter, G. H., and Berz, M., *Proceedings of LHC95, loc. cit.*; Hoffstätter, G. H., Ph.D. Thesis, Michigan State University, 1994.
20. Berz, M., talk at the ITP Conference on Particle Beam Stability and Nonlinear Dynamics, Santa Barbara, California, December 3–5, 1996.
21. Niederreiter, H., *Random Number Generation and Quasi-Monte Carlo Methods*, Philadelphia: SIAM, 1992.
22. Sloan, I. H., and Joe, S., *Lattice Methods for Multiple Integration*, Oxford Univ. Press, 1994.
23. Warnock, R. L., Berg, J. S., and Forest, É., in *Proceedings of the 16th Particle Accelerator Conference (PAC95) and International Conference on High Energy Accelerators*, Dallas, Texas, May 1-5, 1995.